ChemComm

Solvation vs. Surface Charge Transfer: An Interfacial Chemistry Game Drives Cation Motion

Journal:	*ChemComm*
Manuscript ID	CC-COM-03-2021-001408.R1
Article Type:	Communication

COMMUNICATION

Solvation vs. Surface Charge Transfer: An Interfacial Chemistry Game Drives Cation Motion

Stefany Angarita-Gomez and Perla B. Balbuena*

Received 00th January 20xx,
Accepted 00th January 20xx

DOI: 10.1039/x0xx00000x

Electrolyte structure and ion solvation dynamics determine ionic conductivities, and ion (de)solvation processes dominate interfacial chemistry and electrodeposition barriers. We elucidate electrolyte effects facilitating or impeding Li^+ diffusion and deposition, and evaluate structural and energetic changes during the solvation complex pathway from the bulk to the anode surface.

Li metal anodes are one of the most promising anode material choices to fulfil the increasing demand of high energy density batteries.[1-5] However, key factors related to the unstable solid electrolyte interphase (SEI) formation and the uneven lithium nucleation during electrodeposition have hampered the extensive use of Li metal batteries.[6] One of the main obstacles in the path of finding practical solutions to the standing issues is the lack of understanding of the transport and reaction mechanisms at the electrolyte/electrode interface that is extremely reactive, dynamic, and highly dependent on the chemistry and composition of the electrolyte. Electrolytes play a crucial role in battery stability and electrochemical performance. Recent studies have shown significant efforts on electrolyte optimization based on their electrochemical stability window, ionic conductivity, and SEI properties.[7-9] The electrolyte plays important roles in bulk and at the interface. In bulk, the electrolyte's structure and its ion solvation dynamics determine the ionic conductivity that is crucial for fast charge applications. At the interface, the processes of ion (de)solvation dictated by the electrolyte are in control of the interfacial chemistry, along with the reduction kinetics and interfacial transport properties, and also play a key role on the metal plating and stripping processes.[10-12] Hence, there is an urgent need to elucidate how the electrolyte properties affect the events that a solvated Li cation may encounter during its diffusion and deposition pathway. In this Communication, we show that depending on their chemistry and structure, electrolytes may facilitate or impede the diffusion and deposition of the Li cation on the electrode surface. Clear structural and energetic changes in the cation solvation shell from the bulk electrolyte to the anode surface correlate with barriers for ion transport and electroreduction at the surface.

The electrolytes used in this study consist of 1.0 M $LiPF_6$ in different solvents including 1,2-Dimethoxyethane (DME), Ethylene carbonate (EC), 1,3-Dioxolane (DOL), and mixtures of EC with the additive Fluoroethylene Carbonate (FEC 10 mol%) which has been shown effective to enhance SEI stability and improve battery performance.[7, 8] Thermodynamic integration within the Blue Moon ensemble as implemented in VASP [13-16] is used to evaluate the free energy pathway for Li^+ from the bulk region until its deposition on the Li anode surface, based on constrained ab initio molecular dynamics (c-AIMD) simulations. Once the most significant dynamic events are identified at key points of the trajectory, the corresponding enthalpy and entropy contributions are characterized using Gaussian 16. Figures S1 and S2 show the initial configurations for the Li^+ solvation shell in each of the electrolytes. The primary solvation shell of the Li^+ was extracted from density functional theory (DFT) optimized structures to ensure a stable initial solvation shell. A full description of the computational methods implemented in this study are included as Supporting Information.

Figure 1 shows the free-energy profile of the Li^+ transport pathway as a function of a collective variable (ξ) defined as the cation trajectory from an initial point in the bulk electrolyte until a final point on the Li metal surface. Although the initial and final points are pre-defined, the path that the cation takes is determined by its solvation thermodynamics and kinetics, and by interactions with the surrounding environment including electron transfer effects as the surface is approached. The

Department of Chemical Engineering, Texas A&M University, College Station, TX 77843
**E-mail: balbuena@tamu.edu*

† Electronic Supplementary Information (ESI) available: Initial configurations for simulations (Fig. S1 and S2), Full description of computed Gibbs Free Energy of Solvation, Standard Enthalpies and Standard Entropies at 298 K (Table S1), Free energy profile for EC solvent (Fig. S3), Solvation shell description for steps in Fig. S3 (Fig. S4 and S5), Free energy profile for DOL solvent (Fig. S6), Solvation shell description for steps in Fig. S6 (Fig. S7 and S8), Free energy profile for FEC/EC mixtures (Fig. S9), Solvation shell description for steps in Fig. S9 (Fig. S10). See DOI: 10.1039/x0xx00000x

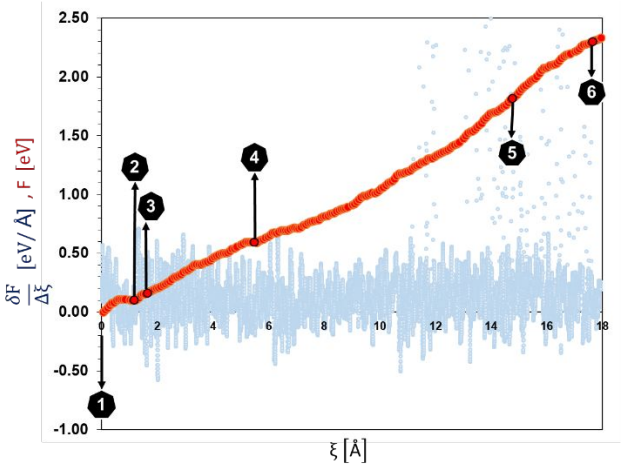

Figure 1. Free-energy profile of lithium cation diffusion and deposition in 1.0 M $LiPF_6$ in DME. Marks 1 through 6 highlight important events along the Li^+ pathway (see text).

	ξ [Å] Reaction Coordinate	F [eV] Free Energy	ΔF [eV] Free Energy change relative to previous step	Description
1	0.00	0.00	0.00	Initial solvation shell includes 3 oxygen atoms from 2 different DME molecules (red)
2	1.16	0.11	0.11	Stable structure after a new DME molecule (blue) becomes part of the solvation shell
3	1.64	0.16	0.05	Solvation shell rearrangement– 3 molecules of DME
4	5.48	0.59	0.43	One DME molecule leaves the shell. Current shell has 2 O atoms from each DME (red, blue)
5	14.76	1.81	1.21	Energy change corresponds to the diffusion of the complex in 4 and the addition of a 3rd DME molecule to the shell (yellow), this step is the beginning stage of the cation deposition
6	17.88	2.32	0.52	DME molecule (blue) left the solvation shell, and the other 2 move with cation until its deposition

Figure 2. Description of events corresponding to energy pathway steps 1 through 6 in Figure 1. Solvation shells are found during the lithium cation (green) diffusion and deposition pathway. Surface Li atoms in purple. Background solvent molecules have all atoms except H in grey, and H atoms in white.

thermodynamic integration method yields the free energy of the system (F) along the reaction coordinate, that results from integrating the differential change in free energy with respect to the change in the reaction coordinate ($dF/d\xi$). The free energy reflects an uphill process, however there are individual events that are identified between minima in the trajectory and are highlighted below. For example, marks 1 through 6 in Figure 1 indicate diffusion and deposition events for the 1.0 M $LiPF_6$ in DME solution. In the bulk electrolyte, although not always successful, the cation seeks its best solvation configuration that minimizes its energy. However, we next show that the driving force offered by the surface changes such pattern. Figure 2 highlights the description of events marked 1 through 6 in Figure 1 along with the energy difference between steps. The initial solvation complex formed by the Li^+ solvated by 2 DME molecules (Figure 2, mark 1) changes structure several times (marks 2, 3, 4) optimizing its configuration while traveling in the direction of the surface.

As a result of the relative stability of the solvation complex in mark 4, Li^+ along with its first shell diffuses towards the metal surface without any structural change. In the vicinity of the surface, DME molecules (e.g. DME shown in yellow, mark 5) are at least partially receiving the surface electron transfer and are able to attract the cation and part of its accompanying shell. Mark 5 represents the beginning of the deposition step of the Li^+ marked by the last new DME addition to the solvation complex as well as the desolvation of other DME molecules (mark 6). In presence of the highly stable DME molecule, it is found that the cation is reduced by electron transfer from the Li metal in the final step.

To fully quantify the changes of solvation enthalpies and entropies during the free energy pathway for Li^+ in $LiPF_6$/DME, we extracted the primary solvation shell of each individual step detected during the c-AIMD simulations (Figure 2) and optimized the solvated structure using B3PW91/6-311++G(d,p) and an implicit solvent. The results are shown in Figure 3. The goal is to obtain additional details regarding the changes in enthalpy and entropy of solvation for every relevant step in the cation's pathway. The cluster calculation confirms that although the initial complex solvation is in a local energy minimum, during its journey towards the surface it experiences other rearrangements in the search for an even lower energy state. By the time the cation reaches mark 4, the solvation shell registers the lowest energy and the longest amount of time during the Li^+ diffusion is spent in this shell configuration. However, surface electron transfer starts to play a role in the next steps attracting the solvation complex. This explains the energy increase from marks 4 to 5 creating a less stable solvation complex. The initial deposition attempts are captured in 6, where the cation is still solvated by two O atoms from DME molecules, but is already interacting with the surface atoms, that take the system to a new local energy minimum. At this point the cation becomes reduced, which requires overcoming an energy barrier. The Li metal atom still interacts with some of the DME molecules, but becomes integrated with a Li metal cluster of 5 atoms representing the slab surface. The addition of this new metal atom to the Li metal slab (mark 6*) has an energy requirement of ~ 0.86 eV, that is the barrier for cation reduction under the open circuit condition of the simulation.

It is very interesting to follow the enthalpic and entropic contributions during the cation evolution free energy pathway. Thermodynamic properties of the Li^+ solvation complex in Figure 3 are highlighted in Table 1. Full details of this calculation are provided in Table S1 in the Supporting Information.

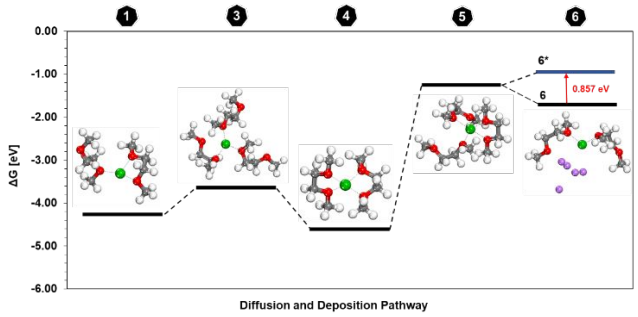

Figure 3. Solvation free energy pathway for lithium cation during the diffusion and deposition pathway in DME solvent at the B3PW91/6-311++G(d,p) level of theory.

Table 1. Changes in thermodynamic properties through the free energy pathway shown in Figure 3. Computed Gibbs Free Energy of Solvation, Standard Enthalpies, and Standard Entropies at 298 K.

Solvation Shell	ΔG [eV]	ΔH [eV]	TΔS [eV]
1	-4.245	-0.464	3.781
3	-3.646	-0.414	3.232
4	-4.593	-0.920	3.673
5	-1.275	-0.785	0.490
6	-1.793	-3.132	-1.339
6*	**-0.936**	**-1.940**	**-1.004**

Standard molar entropies in Table 1 reveal a dominant behavior in the first three solvation configurations, although enthalpy has a small gain in the most stable structure (mark 4). From 4 to 5, there is a clear decrease in the entropy contribution that determines a large free energy barrier from 4 to 5. During the last steps, the negative entropy changes reveal a completely different thermodynamic driving force, now dominated by the enthalpy of surface attraction forces driven by electron transfer. Finally, the last step shows a new entropy increase due to the incorporation of the cation to a new surface ordered state, accompanied by a slight decrease of the enthalpy change. Based on the free energy barriers, it is concluded that for this electrolyte, the rate determining step is given by mass transfer from the electrolyte phase to the surface.

Next, we evaluate the effect of the solvent electron affinity. For this, we turn to a much reactive solvent, EC. The behaviour of the EC-based solvation complex has some interesting dissimilarities with the previous case. The Li^+ pathway of diffusion and deposition and its energy profile are shown in Figure S3, the description of the events are in Figure S4 and Figure S5. Figure S3 shows a much less steep free energy profile than that in Figure 1. This is because, in contrast with the DME solvation complex, the Li^+ solvation shell formed by EC has fewer structural changes during the cation journey towards the surface, with much lower diffusion barriers. Only one molecule is added to the initial solvation shell resulting in a strong stable shell formed by 4 EC molecules (Figure S4). Further, another difference with the DME system appears in the Li+ desolvation and deposition process (Figure S5). Once the solvated complex gets close to the surface, the higher EC electron affinity compared to DME causes a surface-driven alignment structure in the solvent molecules (Mark 5 and 6 in Figure S5). The solvated cation approaches the surface driven by a partially reduced EC molecule (~ -0.11e at mark 6 in Figure S5). The reduction of the solvation complex continues while partial desolvation of the Li^+ can be observed (Mark 8 in Figure S5). However, the cation is not reduced, instead it combines with fragments from EC decomposition becoming part of a new SEI product that is incorporated to the surface.

As a second comparative test, we evaluate the DOL solvent that has a higher electron affinity than DME but is more stable than EC.[17] Compared with the Li^+ pathway in DME and EC the number of highlighted events in Figure S6 suggests a very dynamic DOL-based solvation complex. The solvation shell formed around the Li^+ by the DOL molecules changes rapidly with small energy barriers shown in Figure S7. Figure S8 shows the desolvation and deposition of the cation driven by molecules closer to the metal surface that is partially charged (mark 10 in Figure S8, orange ~ -0.32 e, pink ~ -0.22 e, and turquoise ~ -0.36 e). One by one these molecules desolvate the Li^+ and transfer their charge (Mark 12 Figure S8 Orange ~-0.02 e and pink ~0.14 e). This fast charge transfer by DOL was noticed in a previous study on charged surfaces.[17] As a consequence, the cation is reduced and becomes part of the Li metal surface only interacting with one DOL molecule partially charged with ~ -0.18 e. Thus, DOL behaves similar to DME with a diffusion-limited process.

Finally, we tested an FEC/EC mixture of additive/solvent. The mechanisms of diffusion and deposition in the electrolyte shown in Figure S9 in which the electrolyte is EC with FEC 10 mol% are similar to the pathway of the Li cation in EC. In this electrolyte, the Li^+ solvation complex suffers several structural changes. Initially one of the FEC molecule leaves the shell which stabilizes with EC molecules. However, towards the desolvation stage, the cation drags part of its initial solvation shell including one FEC molecule (mark 5 in Figure S10). This is because FEC has a higher reduction potential than EC and therefore it is more likely to be found near the surface. Similar to the case EC, the cation is not reduced and instead it becomes part of the nascent SEI on the surface formed by reduced EC molecules.

The ability to differentiate between cation diffusion, desolvation, and deposition pathway for different electrolytes allows a fundamental understanding of the Li^+ pathway and the barriers arising in each electrolyte for transport and electrodeposition of the cation on the surface. Figure 4 shows that desolvation is more difficult for DME and DOL than for EC and EC/FEC. In solvents with low reduction potential (low electron affinity) such as DME and DOL[18] the barriers for ion transport are determined by reorganization of molecules in the primary solvation shell.

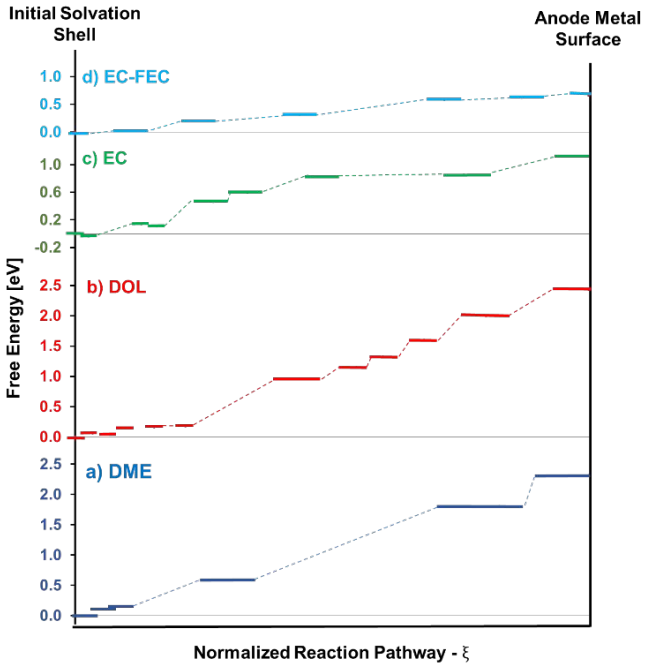

Figure 4. Comparison of Free-energy profile of lithium cation diffusion and deposition in 1.0 M $LiPF_6$ for different electrolytes a) DME, b) DOL, c) EC , and d) EC-FEC.

Thus, for these relatively stable solvents, mass transfer is limited by entropic forces that keep well-ordered solvation shells. Upon reaching the surface, enthalpic contributions arise from cation interactions with negatively charged surfaces that facilitate cation desolvation and reduction by electrons from the Li metal surface. In solvents with higher reduction potential such as EC and FEC, the solvation complex prefers to travel alongside the cation, limiting the shell structural changes as shown in Figure 4c and 4d. Close to the surface, the alignment of the solvent molecules following the cation towards the surface is more preferred than the cation complete desolvation. In the final stage, partially reduced molecules drag the complex including the cation that becomes part of the SEI. In summary, this work quantifies electrolyte effects on the thermodynamics and kinetics of ion transport and deposition on Li surfaces, which are key for identifying rates of battery charge and plating phenomena. Competition between solvation forces keeping stable structures and electron transfer from the surface attracting electrophilic species exists at any point in the ion trajectory, particularly as the ion approaches the surface, and would be naturally influenced by a surface with an excess charge.[17, 19] Future work will demonstrate this analysis for charged surfaces, high concentrated and localized-concentrated electrolytes and surfaces with incipient metal nucleation.

All authors have given approval to the final version of the manuscript. S. A.-G. performed all the computations and analysed the outputs from first-principles simulations. P.B.B. originated the idea, and supervised the work. S.A.-G. and P.B. B. discussed and interpreted the results, and contributed to the preparation of the manuscript.

This work was supported by the U.S. Department of Energy's Office of Energy Efficiency and Renewable Energy (EERE), as part of the Battery 500 Consortium, Award Number DE-EE0008210. Supercomputer resources from the Texas A&M University High Performance Computer Center and from Texas Advanced Computing Center (TACC) are gratefully acknowledged.

There are no conflicts to declare.

1. C. Fang, X. Wang and Y. S. Meng, *Trends in Chemistry*, 2019, **1**, 152-158.
2. J. B. Goodenough and Y. Kim, *Chemistry of Materials*, 2010, **22**, 587-603.
3. X. Chen, T. Hou, K. A. Persson and Q. Zhang, *Materials Today*, 2019, **22**, 142-158.
4. J. Lai, Y. Xing, N. Chen, L. Li, F. Wu and R. Chen, *Angewandte Chemie International Edition*, 2020, **59**, 2974-2997.
5. D. Lin, Y. Liu and Y. Cui, *Nature Nanotechnology*, 2017, **12**, 194.
6. L. Fan, H. L. Zhuang, W. Zhang, Y. Fu, Z. Liao and Y. Lu, *Advanced Energy Materials*, 2018, **8**, 1703360.
7. T. Hou, G. Yang, N. N. Rajput, J. Self, S.-W. Park, J. Nanda and K. A. Persson, *Nano Energy*, 2019, **64**, 103881.
8. B. Liu, W. Xu, P. Yan, S. T. Kim, M. H. Engelhard, X. Sun, D. Mei, J. Cho, C.-M. Wang and J.-G. Zhang, *Advanced Energy Materials*, 2017, **7**, 1602605.
9. X.-Q. Zhang, X. Chen, X.-B. Cheng, B.-Q. Li, X. Shen, C. Yan, J.-Q. Huang and Q. Zhang, *Angewandte Chemie International Edition*, 2018, **57**, 5301-5305.
10. A. Baskin and D. Prendergast, *The Journal of Physical Chemistry Letters*, 2020, **11**, 9336-9343.
11. R. Attias, M. Salama, B. Hirsch, Y. Goffer and D. Aurbach, *Joule*, 2019, **3**, 27-52.
12. N. Tanibata, R. Morimoto, K. Nishikawa, H. Takeda and M. Nakayama, *Analytical Chemistry*, 2020, **92**, 3499-3502.
13. G. Kresse and J. Furthmuller, *Computational Materials Science*, 1996, **6**, 15-50.
14. G. Kresse and J. Hafner, *Physical Review B*, 1993, **47**, 558.
15. G. Kresse and J. Hafner, *Physical Review B*, 1994, **49**, 14251-14269.
16. T. Bucko, *Journal of Physics: Condensed Matter*, 2008, **20**, 064211.
17. L. E. Camacho-Forero and P. B. Balbuena, *Journal of Power Sources*, 2020, **472**, 228449.
18. J. Han, Y. Zheng, N. Guo and P. B. Balbuena, *The Journal of Physical Chemistry C*, 2020, **124**, 20654-20670.
19. R. C. Longo, L. E. Camacho-Forero and P. B. Balbuena, *Journal of Materials Chemistry A*, 2019, **7**, 8527-8539.